

Wave Ducting in a Stratified Shear Flow over a Two-Dimensional Mountain. Part II: Implications for the Development of High-Drag States for Severe Downslope Windstorms

TING-AN WANG* AND YUH-LANG LIN

Department of Marine, Earth and Atmospheric Sciences, North Carolina State University, Raleigh, North Carolina

(Manuscript received 26 August 1996, in final form 20 March 1998)

ABSTRACT

In this study, it is found that the discrepancies among earlier studies of severe downslope windstorms are caused by the use of the critical level height (z_c), instead of the low-level uniform flow-layer depth (z_1), as an indicator to determine the optimal conditions for the occurrence of high-drag states. It is determined that once the wave breaking occurs, it induces a critical level and establishes a flow configuration favorable for wave ducting in the lower uniform wind layer, which determines the phase of reflected waves.

Flow regimes of high- and low-drag states for a two-dimensional, nonrotating flow with uniform static stability and a basic-state critical level over a mountain were also determined as functions of nondimensional mountain height (\bar{h}), Richardson number (Ri), and nondimensional z_1 in the terrain-following coordinates ($\bar{\sigma}_1$). The authors found that 1) the critical \bar{h} for high-drag state increases as Ri increases when $\bar{\sigma}_1$ is fixed, 2) the critical \bar{h} for high-drag state increases as $\bar{\sigma}_1$ increases from $0.175 + n$ to $1.175 + n$ when Ri is fixed, and 3) the low-level response repeats periodically at one vertical wavelength. It was found that the nonlinear and critical level effects make the selection of high-drag states ($\bar{\sigma}_1 = 0.175 + n$) from the linear wave duct modes ($\bar{\sigma}_1 = 0.175 + n/2$). If a very stable layer is induced above $\bar{\sigma}_1$, then the linear wave duct mode tends to be suppressed and the flow cannot develop into a high-drag state because the wave-ducting structure is destroyed. On the other hand, if a strong unstable layer is induced above σ_1 , then the linear wave duct mode may further develop into a high-drag state.

Therefore, it is proposed that the development of a high-drag or severe wind state is supported by the nonlinear wave-ducting mechanism, whereas the high-drag state at the mature stage is maintained by the hydraulic mechanism as proposed by some earlier studies. It was found that nonlinearity plays an essential role in the downward and downstream expansion of the turbulent mixing region during the development stage of a severe downslope windstorm, which forces the fluid below this region to accelerate and propagate downstream as a hydraulic jump.

1. Introduction

Severe downslope windstorms over the lee of a mountain ridge have been observed in various places around the world, such as the chinook over the Rocky Mountains, the foehn over the Alps, the bora over the Yugoslavian coastal mountain range, and the zonda in Argentina. One well-documented case is the 11 January 1972 windstorm that occurred in Boulder, Colorado (Lilly and Zipser 1972; Lilly 1978). Intense and damaging surface winds arise in the lee of mountains when these

low-level waves attain large amplitude (Klemp and Lilly 1975). The dynamics of severe downslope windstorms has been studied extensively in the last three decades. Three major mechanisms have been proposed to explain the formation of severe downslope windstorms: 1) the partial reflection mechanism (Klemp and Lilly 1975), 2) the resonant amplification mechanism (Peltier and Clark 1979, 1980; Clark and Peltier 1984, hereafter CP84), and 3) the hydraulic mechanism (Smith 1985, hereafter S85). Predictions of S85's theory have been confirmed by numerical model simulations (Durran 1986; Durran and Klemp 1987, hereafter DK87; Bacmeister and Pierrehumbert 1988, hereafter BP88) and by tank experiments (Rottman and Smith 1989).

Based on linear, hydrostatic mountain wave theories, Klemp and Lilly (1975) proposed that strong amplification of severe downslope winds is associated with the optimal superposition of upward- and downward-propagating waves. The downward-propagating waves are produced by partial reflection from interfaces of a mul-

* Current affiliation: Research Scientist, Civil Aeronautics Administration, Taipei, Taiwan.

Corresponding author address: Prof. Yuh-Lang Lin, Department of Marine, Earth and Atmospheric Sciences, North Carolina State University, Raleigh, NC 27695-8208.
E-mail: yl.lin@ncsu.edu

tilayered atmosphere. A low-level stable layer and the partial reflection from the tropopause often play important roles in generating large-amplitude waves. They found that an optimal tuning occurs when the tropopause is located at one-half vertical wavelength ($\frac{1}{2}\lambda$) above the ground. However, the wave shift and reflection coefficient for wave resonance predicted by their linear theory becomes less accurate for flow over a finite-amplitude mountain.

From nonlinear numerical model simulations, Peltier and Clark (1979, 1983) found that a high-drag or severe wind state may be established after the upward-propagating mountain waves break. The wave-breaking region is characterized by strong turbulent mixing, with a local wind reversal on top of it. This wind reversal level is also called the “wave-induced critical level” by them. Note that critical level is defined as the level at which the mean wind speed coincides with the phase speed of the wave. For a stationary mountain wave, the critical level coincides with the wind reversal level because the phase speed there is zero. They proposed that the wavebreaking region aloft acts as an internal boundary that reflects the upward-propagating waves back to the ground and produces the high-drag state through partial resonance with the upward-propagating mountain waves. In a way this is roughly parallel to Klemp and Lilly’s partial reflection mechanism, although the nonlinearity has been included in Peltier and Clark’s model and the wave-induced critical level serves as the reflecting boundary. Peltier and Clark (1983) suggested that the severe wind state will develop if the critical level is located at a height of $(\frac{3}{4} + n/2)\lambda$, where $n = 1, 2, 3, \dots$ and $\lambda = 2\pi U/N$ is the hydrostatic vertical wavelength and U and N are wind speed and Brunt-Väisälä frequency. They then conducted a series of numerical experiments with the critical level located at different heights to investigate the mechanisms of severe downslope windstorms. Later, Clark and Peltier (1984, denoted as CP84 hereafter) proposed that there is no dependence of the initial wave-breaking height on nondimensional mountain height; that is, it always occurs near $\frac{3}{4}\lambda$. They then claimed that these results strongly support their resonance theory.

Based on Long’s (1953) nonlinear theory for uniform flow over a finite-amplitude mountain, S85 developed a mathematical theory of the severe wind state. This theory assumes that the density of the fluid in between the divided streamlines is uniform, and above the upper dividing streamline the fluid is essentially quiescent. This assumption is based on the observational and numerical experimental evidence that during severe downslope windstorms, a large region of well-mixed, slow turbulent air develops in the middle and upper troposphere while strong winds plunge underneath. He proposed that the severe downslope wind state occurs due to the interaction between a strong smoothly stratified flow and this deep turbulently mixed “dead” region. This mechanism is also called the hydraulic mechanism

because the flow structure mimics the classical one- or two-fluid hydraulic model (e.g., Long 1954; Houghton and Kasahara 1968). In contradiction with CP84, this theory predicted that the severe wind state exists over the entire range of critical level height between $(\frac{3}{4} + n)\lambda$ to $(\frac{3}{4} + n)\lambda$. In addition, the critical level for a severe wind state depends on the nondimensional mountain height and its height is an intrinsic property of the severe wind configuration. DK87 and BP88 have performed a series of numerical experiments and confirmed Smith’s theory (S85). Smith’s theory appears to be able to accurately predict the altitude of the turbulent air, the strength of the downslope winds, and the mountain drag, and thus has significantly advanced our understanding of the dynamics of severe downslope windstorms. However, S85’s theory is primarily a consistency analysis of a severe wind configuration and provides little help in making prediction of when the severe wind state will occur (S85).

Although the wave-breaking height ($\bar{z} = \frac{3}{4} + n/2$) is different from that predicted by S85’s theory, it may represent the wave-breaking level at a different stage. Based on a weakly nonlinear theory, Grimshaw and Smyth (1986) showed that the initiation of a high-drag transitional flow begins with linear resonance. In addition, Lin and Wang (1996) showed numerically that the initial overturning level in a two-dimensional, nonrotating, uniform flow over a mountain ridge is almost equal to $\frac{3}{4}\lambda$, which is consistent with that predicted by CP84’s linear resonance theory and by nonlinear numerical models (e.g., Laprise and Peltier 1989b). Thus, one may hypothesize that the critical level height for a severe wind state to exist starts from the wave-breaking level at early stage but is modified by the nonlinearity when the flow develops into a high-drag state. In other words, at the early stage of severe wind development, the flow is dominated by the nonlinear wave-ducting mechanism, whereas the flow is dominated by hydraulic dynamics at a later stage. A complete understanding of the wave breaking is important for making the prediction of when the severe wind state will occur.

In above-mentioned studies of severe downslope windstorms, the nondimensional critical level height (\bar{z}_c) is used as an indicator to determine the high-drag states. Based on the linear theory developed in Part I, \bar{z}_c with the strongest low-level response is strongly dependent on the Richardson number (Ri) (Fig. 5 of Part I), whereas the nondimensional depth of the lower uniform flow layer (\bar{z}_1) with the strongest low-level response is almost independent of Ri when N is uniform or $N_2/N_1 \ll 1$ (Figs. 4a and Fig. 6c of Part I, respectively). It is also found in Part I that \bar{z}_c plays a dominant role in the phase of the reflected waves. This implies that \bar{z}_1 may serve as a better parameter than the nondimensional critical level height (\bar{z}_c) as an indicator to determine the optimal condition for the occurrence of high-drag states, such as that adopted in earlier studies. Based on the linear wave-ducting theory developed in Part I and nonlinear

modeling simulations, we will try to use this new parameter to examine the results from a number of earlier studies of severe downslope windstorms and to clarify the discrepancies between them.

In the wave-breaking region, the static stability is significantly reduced because the air there is well mixed. This, in turn, will give a very low Richardson number in the wave-breaking region or the dead region as described by S85. With the wave-induced critical level and the resulting structure of static stability and horizontal wind velocity, the flow configuration is similar to that of Lindzen and Tung (1976, hereafter LT76). This type of flow configuration has also been depicted in Fig. 1 of Part I (Wang and Lin 1998) of this series of papers, which is also similar to that in CP84, but with a constant shear and low Brunt–Väisälä frequency in the middle layer. BP88 has adopted the same wind profile, but with no variation in Brunt–Väisälä frequency. As reviewed in Part I, LT76 showed that the lower stable layer adjacent to the surface may serve as a wave duct under certain conditions. For example, a wave duct may exist if the lower stable layer is capped by a dynamically unstable layer with $Ri < 1/4$ and the duct has a depth of $(1/4 + n/2)\lambda$. LT76's linear wave-ducting mechanism was extended to more general linear criteria in Part I. In this study, we hypothesize that the wave-ducting mechanism may help the flow to develop from the onset of wave breaking into a severe wind state.

Scinocca and Peltier (1993), using a triple-nested-grid numerical model initialized with Long's analytical solution, identified three distinct stages for the development of downslope windstorms. In the first stage, local convection acts to neutralize the region of overturned streamlines, producing a pool of well-mixed fluid aloft. In the second stage of development, a well-defined large-amplitude stationary disturbance is generated over the lee slope. In time, small-scale secondary Kelvin–Helmholtz (K–H) (shear) instability develops in local regions of enhanced shear associated with flow perturbations caused by the large-amplitude disturbance. During the third stage of development, the region of enhanced wind on the lee slope expands in the downstream direction, eliminating the perturbative structure associated with the large-amplitude stationary disturbance. Shear instability comes to dominate the flow in the mature windstorm state. The analysis by Laprise and Peltier (1989a,b) and Scinocca and Peltier (1993) provides some physical insights into the detailed structure of the flow response at each stage of development of severe downslope windstorms. In this study, we will apply the wave-ducting mechanism to explain the second and third stage of severe downslope winds as proposed by Scinocca and Peltier (1993).

The objectives of this study are to 1) clarify the discrepancies among various studies of severe downslope windstorms, 2) investigate the nonlinear and critical level effects on the selection of high-drag states from linear wave duct modes, and 3) apply the nonlinear wave-

ducting mechanism to the development of high-drag states associated with severe downslope windstorms. Both linear theory and systematic nonlinear numerical simulations will be used in this study. The linear analysis is based on the wave-ducting theory developed in Part I. The paper is organized as follows. The numerical model is briefly described in section 2. Section 3 discusses the sensitivity of the low-level response to the height of the basic-state critical level and the depth of the lower uniform flow layer. The nonlinear effects on the selection of linear wave duct modes into high-drag states will be studied in section 4. In section 5, the nonlinear wave-ducting mechanism will be applied to the formation of high-drag states associated with severe downslope windstorms. The concluding remarks can be found in section 6.

2. The nonlinear numerical model

To answer the questions addressed in the introduction, we adopt the simple nonlinear numerical model used by Lin and Wang (1996). This two-dimensional, hydrostatic version of the North Carolina State University geophysical fluid dynamics model integrates the nonlinear primitive equations governing orographically forced finite-amplitude perturbations in a uniform, nonrotating, stratified, hydrostatic, Boussinesq flow. A brief summary of this model can be found in Part I of this study, and the details are given in Lin and Wang (1996) and Weglarz (1994). To simulate flow over mountains, a terrain-following vertical coordinate is adopted in the model. The vertical coordinate is defined as $\sigma = z_t(z - z_s)/(z_t - z_s)$, where z_s is the surface height and z_t is the top of the computational domain. Thus, the governing equations are expressed in the (x, σ) space, instead of in the (x, z) space. In analyzing the numerical results from terrain-following models, these effects need to be taken into consideration in comparing with the results predicted by a linear theory in the (x, z) domain. For example, in a linear theory, the lower boundary condition is applied at $z = 0$. Thus, the height of the lower layer (z_l) for strongest low-level responses in a two-dimensional, nonrotating, continuously stratified flow over an isolated mountain predicted by the linear theory should be taken as σ_1 in an (x, σ) coordinate system because the lower boundary condition is applied at the terrain surface ($\sigma = 0$).

3. Sensitivity of low-level response on \tilde{z}_l and \tilde{z}_c

One of the questions we would like to address is whether \tilde{z}_c (the wave-induced critical level) is an appropriate indicator to determine the optimal conditions for the occurrence of high-drag states or not. As discussed in the introduction, we propose to use \tilde{z}_1 (the depth of the lower uniform wind layer) as the indicator because the phase of the reflected waves is primarily determined by \tilde{z}_1 (Part I). To study this problem, we

performed a series of systematic experiments with a three-layer flow configuration as shown in Fig. 1 of Part I. The results are shown in Fig. 1 in the present paper. The parameters used in these experiments are similar to those used in DK87 where $N_1 = N_2 = N_3 = 0.01047 \text{ s}^{-1}$, $U_1 = 20 \text{ m s}^{-1}$, $U_3 = 0 \text{ m s}^{-1}$, $U_c = 0.01 \text{ s}^{-1}$, $z_c - z_1 = 2 \text{ km}$, and $z_2 = z_c$. The Ri associated with this flow is about 1.0. There are three sets of experiments with $\tilde{h} = 1/\text{Fr} = N_1 h/U_1 = 0.714, 0.5, 0.333$, respectively, where Fr is the Froude number. For each set of experiments, the nondimensional depth above the mountain peak of the uniform wind layer in the terrain-following coordinates ($\tilde{\sigma}_1$) varies from 0.125 to 1.5, where $\tilde{\sigma}_1$ is normalized by $2\pi U_1/N_1$. The surface drag, normalized by $\pi\rho U_1 N_1 h^2/4$, is shown in Fig. 1a. The results in Fig. 5 of CP84, Fig. 2 of BP88, and Table 1 of DK87 are also plotted. As previously stated, they used \tilde{z}_c as an indicator to determine the optimal conditions for the occurrence of high-drag states.

As mentioned earlier, we hypothesize that the wave-ducting mechanism plays important roles in the formation of high-drag states associated with severe downslope windstorms. If this is true, then the height of the lower uniform wind layer (\tilde{z}_1) is a better indicator than the critical level height (\tilde{z}_c). In the terrain-following coordinates, the transformation factor needs to be considered. Thus, the depth of the lower uniform wind layer over the mountain peak in the terrain-following coordinates ($\tilde{\sigma}_1$) should be a better indicator than $\tilde{\sigma}_c$. The use of $\tilde{\sigma}_1$ is also necessary for comparing results from linear theory (in which the lower boundary is applied at $z = 0$) and nonlinear terrain-following numerical models. Note that these heights ($\tilde{\sigma}_c$ and $\tilde{\sigma}_1$) do not correspond directly to the upstream (H_0) or downstream (H_1) dividing streamline height in S85's model. A careful inspection of the isentropes of the 1972 Boulder windstorm (Lilly 1978) shows that the top of the lower layer does start to descend from above the mountain peak (i.e., the continental divide). Similar results can also be found from nonlinear numerical simulations, such as Fig. 28 of Peltier and Clark (1979) and Fig. 10 of Durran (1986). The relationship between $\tilde{\sigma}_1$ and \tilde{z}_c may be written

$$\tilde{\sigma}_1 = \frac{\tilde{z}_c - \tilde{b} - \tilde{h}/2\pi}{1 - \tilde{h}/(2\pi\tilde{z}_1)}. \quad (1)$$

The tildes denote nondimensional values, where b is $z_c - z_1$ in the uniform shear case used in this study and DK87 or the half-width of the shear layer in a hyperbolic tangent wind profile used in CP84 and BP88. We define the high-drag state, based on the flow structure from the numerical results (not shown), as those with a normalized surface drag greater than 2. Assuming $\tilde{h}/2\pi \ll \tilde{z}_1$, it may be derived that $\tilde{\sigma}_1$ is related to \tilde{z}_1 and \tilde{h} by the following relationship:

$$\tilde{\sigma}_1 = \tilde{z}_1 - \tilde{h}/2\pi. \quad (2)$$

For convenience, the tildes will be dropped in the rest of text except in the concluding remarks.

The quasi-steady-state normalized surface wave drag as a function of σ_1 and z_c from the present nonlinear model simulations is shown in Figs. 1a and 1b, respectively. Figure 1a indicates that high-drag states exist for $\sigma_1 = 0.125, 0.25, 1.25, 1.375$, and $h = 0.333$ (curve with closed squares); $\sigma_1 = 0.125, 0.25, 0.375, 1.25, 1.375$, and $h = 0.5$ (open squares); and $\sigma_1 = 0.125, 0.25, 0.375, 0.5, 1.25, 1.375, 1.5$, and $h = 0.714$ (closed circles). Results from other nonlinear numerical simulations, such as CP84, DK87, and BP88, have also been plotted using the new control parameter (σ_1). It appears that the predictions of both high- and low-drag states from CP84, DK87, BP88, and the present model by using σ_1 as the control parameter are consistent. Thus, the use of the lower-layer depth appears to better follow a more consistent pattern. This also provides evidence that a wave-ducting mechanism plays an important role in producing high-drag states. In addition, this may imply that discrepancies among the above-mentioned studies are due to a choice of different Ri (2.25 for CP84 vs 1.0 for DK87 and BP88) as well as different velocity profiles (tanh in CP84 and BP88 vs piecewise linear in DK87). In fact, this dependence of flow response to Ri has also been discussed by Scinocca and Peltier (1991), Durran (1993), and Peltier (1993).

In Fig. 1a, when $\sigma_1 = 0.5$, the high-drag state exists for $h = 0.714$, but not for $h = 0.5$. This was explained as a "resonant shift" by BP88. However, we interpret it in a different way. Based on the linear wave-ducting theory developed in Part I, the strongest low-level response occurs when $\sigma_1 = 0.175 + n/2$, $n = 0, 1, 2, \dots$ for $\text{Ri} > 1$. As σ_1 increases from $0.175 + n/2$ to $0.675 + n/2$, the low-level response weakens and the critical nondimensional mountain height (h) for wave breaking increases. According to our results, all cases with $h > 0.2$ and $\sigma_1 = 0.125, 0.25$ belong to high-drag states, which is consistent with the results of other studies (Fig. 1a). However, for $\sigma_1 = 0.375$, a high-drag state occurs only when $h > 0.4$, whereas for $\sigma_1 = 0.5$, it requires $h > 0.7$. This h may be called the critical h for a particular σ_1 . This tendency may also be applied to cases with $\sigma_1 > 1.25$, where the critical h increases as σ_1 increases to the next optimal σ_1 . According to linear theory, the strongest response should repeat itself every half vertical wavelength for a given Ri. Another question may be raised: why does the high-drag state disappear for $\sigma_1 = 0.675$? This absence of a high-drag state may pose a major problem in applying the linear wave-ducting theory to explain the formation of high-drag states associated with severe downslope windstorms. In fact, this question is related to the nonlinear effects in the presence of a basic-state critical level. This will be discussed in section 4. Here we focus on resolving the question of whether z_c is an appropriate indicator to determine the optimal conditions for the occurrence of high-drag states or not.

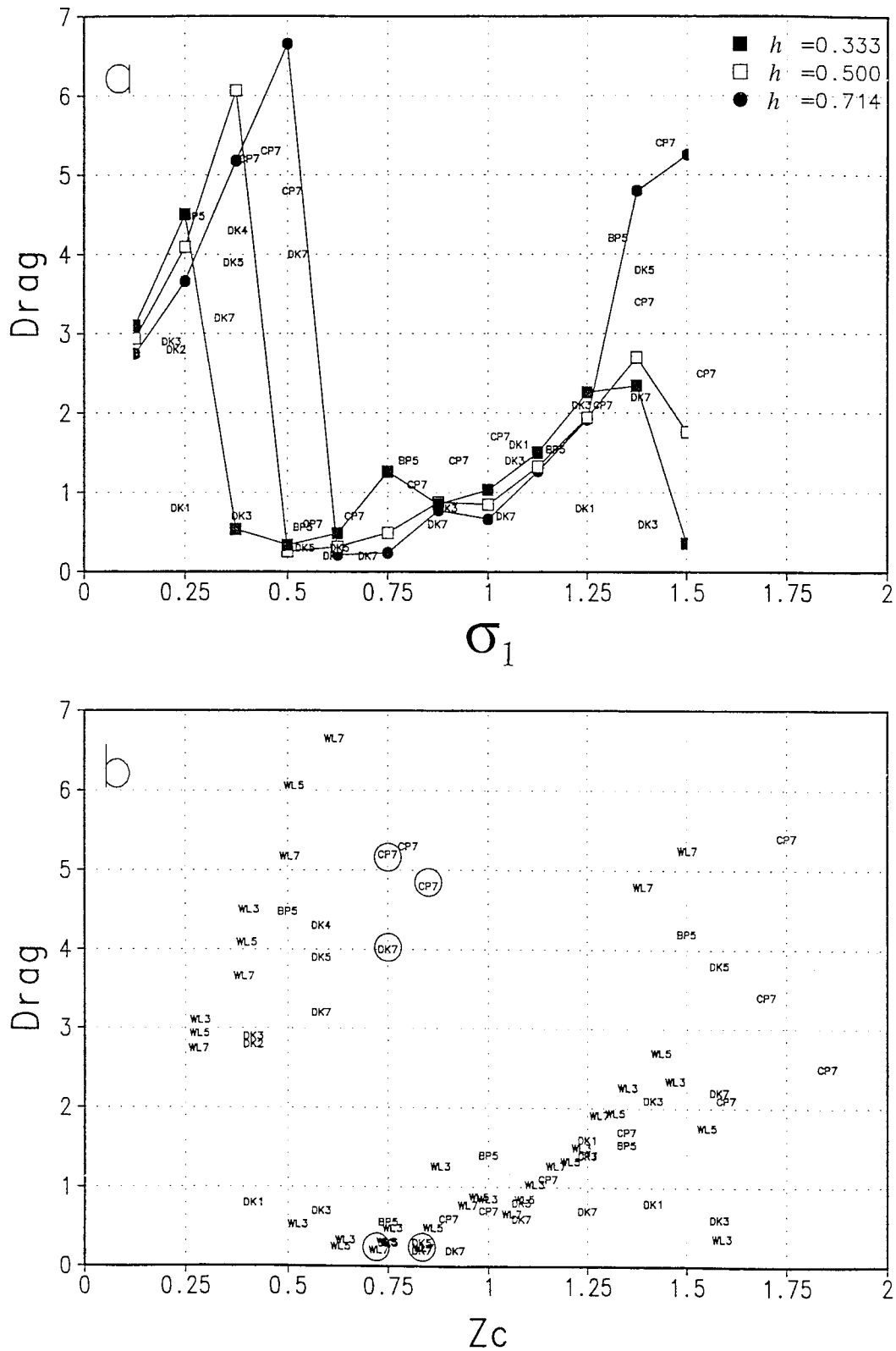


FIG. 1. Steady-state normalized surface wave drag as a function of (a) the nondimensional z_1 in terrain-following coordinates (σ_1) and (b) the nondimensional critical-level height z_c . Here, CP, DK, BP, and WL denote the results from CP84, DK87, BP88, and the present model (Wang and Lin), respectively. The number after DK and WL indicates the value of h . The Ri is 1.0 in these experiments.

Figure 1b shows the quasi-steady-state normalized surface drag, similar to Fig. 1a, except using the non-dimensional critical-level height (z_c) as the independent variable instead of σ_1 . Note that z_c has been used by the aforementioned authors (e.g., CP84, S85, DK87, and BP88) as an indicator to determine the occurrence of high-drag states associated with severe downslope windstorms. There exist numerous discrepancies among these results. For example, when $z_c = 0.85$, a high-drag state (drag = 4.8) exists for $h = 0.75$ in CP84, but it is a low-drag state (drag = 0.2) for $h = 0.7$ in DK87. Another example is that when $z_c = 0.75$, both CP84 ($h = 0.75$) and DK87 are at high-drag states for $h = 0.7$ (drag = 5.2 and 4.0), but our result (denoted as WL in the figure) for $h = 0.714$ is at a low-drag state (drag = 0.2). Another major feature in Fig. 1b is that the high-drag state can occur in a very wide range of z_c , instead of only being possible when $z_c = \frac{3}{4} + n$, $n = 0, 1, 2, \dots$ as proposed by CP84. Based on the above results, our explanation is that once the wavebreaking occurs, it induces a critical level and establishes a flow configuration favorable for wave ducting in the lower uniform wind layer. Thus, the low-level flow response is sensitive to the lower-layer height, instead of the critical-level height. This, in turn, implies that *using the depth of the lower uniform wind layer is a better indicator than the critical-level height to determine the optimal conditions for the occurrence of high-drag states.*

Before proceeding, one may wonder if these critical h curves (Fig. 1a) for different σ_1 can be applied to all nonrotating flow with a basic-state critical level over a two-dimensional mountain. Because all of these results are obtained for $Ri = 1$, except in CP84 where $Ri = 2.25$, the answer is no. According to the linear wave-ducting theory developed in Part I, the low-level flow response is dependent on both Ri and $z_1(\sigma_1)$. As mentioned earlier, the dependence of low-level flow response on Ri has also been found by Scinocca and Peltier (1991). For example, for $Ri > 0.25$ and fixed σ_1 , the magnitude of the strongest low-level response decreases as Ri increases. Therefore, the conclusions from Fig. 1a apply only for a given Ri . To verify the results obtained from our linear wave-ducting theory and to generalize the criteria of critical h for determining high-drag states, we performed more nonlinear numerical simulations for a relatively wider range of Ri . Because $Ri = (N_2/U_2)^2$, and the atmosphere is assumed to be unstructured (N is constant), Ri is totally controlled by wind shear (U_2). The effects of a structured atmosphere will be discussed in a separate study. Figure 2 shows the flow regimes of high- and low-drag states for basic wind with a critical level over a two-dimensional mountain ridge. We use four different values of $\sigma_c - \sigma_1$ ($\approx z_c - z_1$): 0.125, 0.25, 0.375, and 0.5. When σ_1 is fixed in each set of experiments, the corresponding Ri 's are about 0.62, 2.47, 5.55, and 9.87. A curve that separates the high-drag (denoted by circles) and low-drag (denoted by crosses) states is drawn in each panel.

In Fig. 2a ($\sigma_1 = 0.125$), the flow may be characterized as a high-drag state even for very low mountain (e.g., $h = 0.1$) when Ri is small. For example, all cases are in high-drag states when $Ri = 0.62$. Note that the smallest h is only 0.1, which represents a very small-amplitude mountain. Note that it belongs to a high-drag state regime even for such a low mountain when $Ri = 0.62$. When $Ri = 2.47$, the critical h increases to be between 0.1 and 0.2. For $h = 0.1$, the flow belongs to a low-drag state when $Ri = 2.47$, instead of high-drag state when $Ri = 0.62$. As Ri increases further, the critical h for a high-drag state also increases. For $Ri = 5.55$, the critical h falls between 0.2 and 0.3, and when $Ri = 9.87$, it falls between 0.3 and 0.4.

Figure 2b shows the flow regime diagram for $\sigma_1 = 0.25$. Similar to Fig. 2a, the critical h for high drag increases as Ri increases. Overall, the critical h is higher than those in Fig. 2a ($\sigma_1 = 0.125$). This trend of increasing critical h with increasing Ri continues for $\sigma_1 = 0.375$ (Fig. 2c). The critical h for $Ri = 9.87$ is between 0.6 and 0.7. This critical h is only slightly lower than 0.85, which is the critical h for a high-drag state to occur in a uniform, nonrotating, stratified flow over a two-dimensional mountain ridge (Miles and Huppert 1969). This is consistent with the conclusion we drew earlier in this section. That is, when σ_1 increases from $0.175 + n/2$ to $0.675 + n/2$, the critical mountain height (h) for high-drag state increases.

The flow regime undergoes a dramatic change when σ_1 increases to 0.5 and 0.75 (Figs. 2d and 2e). In Fig. 2d, the high-drag flow state exists only for $Ri = 0.62$ and $Ri = 2.44$ when $h = 0.7$. For $Ri = 5.55$ and 9.87, the flow belongs to low-drag states when $h = 0.8$ (≈ 0.85). In Fig. 2e, there exist no high-drag states at all when $h = 0.8$. When $\sigma_1 = 1.25$ (Fig. 2f), the regime diagram is identical to that of $\sigma_1 = 0.25$ (Fig. 2b). Note that for $\sigma_1 = 1.25$, the lower uniform wind layer contains more than a vertical wavelength of the low-level flow. To make comparison, results of CP84, DK87, and BP88 are also replotted in Fig. 2, where h and l denote the high- and low-drag states, respectively. Their results are completely consistent with ours. Therefore, we may conclude that for a nonrotating flow with uniform N and a basic-state critical level over a two-dimensional mountain: 1) The critical nondimensional mountain height (h) for high-drag state increases as Ri increases when σ_1 is fixed, 2) the critical h for high-drag state increases as σ_1 increases from $0.175 + n$ to $1.175 + n$ when Ri is fixed, and 3) the low-level response repeats periodically at one vertical wavelength. This also provides evidence that the wave ducting has played an important role in generating high-drag states.

S85 solved the nonlinear, hydrostatic Long's equation for flow beneath a well-mixed wave-breaking region in a high-drag state. The flow configuration of a quasi-steady, high-drag state observed in the real atmosphere (Lilly 1978) and simulated by numerical models (e.g., Peltier and Clark 1979; Durran and Klemp 1983) is

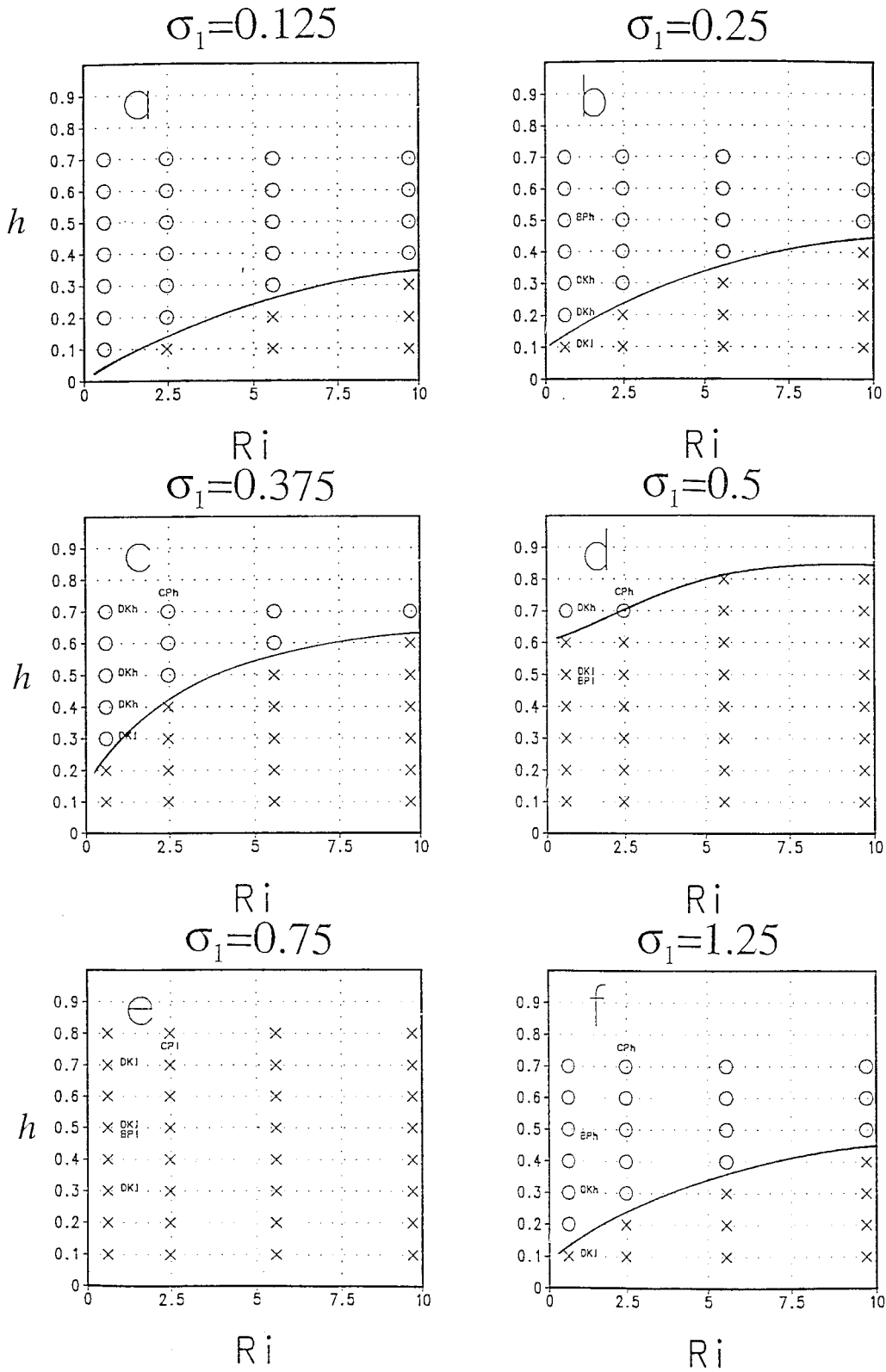


FIG. 2. The flow regime chart in $Ri-h$ map for the cases with (a) $\sigma_1 = 0.125$, (b) $\sigma_1 = 0.25$, (c) $\sigma_1 = 0.375$, (d) $\sigma_1 = 0.5$, (e) $\sigma_1 = 0.75$, and (f) $\sigma_1 = 1.25$. Circle and cross denote high- and low-drag state flow, respectively. CP, BP, and DK have the same meaning as in Fig. 1 and the letters h and l after those denote the high- and low-drag state flow, respectively.

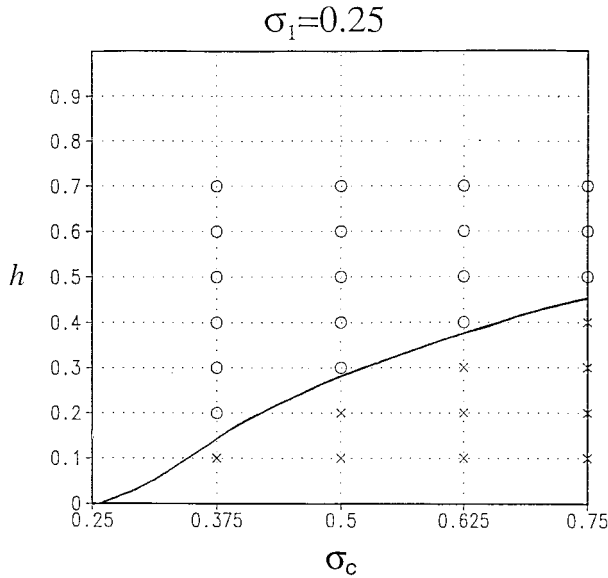


FIG. 3. The relationship of critical nondimensional mountain height h and σ_c when $\sigma_1 = 0.25$, as predicted by the current model simulations.

idealized. In S85's model, the well-mixed region above the layer of severe downslope wind is unspecified. By assuming negligible disturbance above this well-mixed region, the flow fields could be inferred along the lower dividing streamline (i.e., the lower bounding streamline). Imposing this streamline as an upper boundary in the problem, the flow below the well-mixed (stagnant) region could then be determined. A regime diagram of the nondimensional mountain heights (h) and upstream height of the dividing streamline for a high-drag state to occur, is then constructed in his Fig. 5 (S85). According to that regime diagram, the critical h for high-drag state increases as the initial height of the dividing streamline (denoted as \hat{H}_0 in S85) increases. S85's theory is confirmed numerically by DK87 and BP88. To examine the present wave-ducting mechanism, we perform several numerical simulations with $\sigma_1 = 0.25$. Figure 3 shows that the critical nondimensional mountain height (h) for high-drag state increases as the critical level height (σ_c) increases. For small $\sigma_c - \sigma_1$, such as from 0 to 0.125, the present result agrees well with S85's Fig. 5, if his upstream and downstream heights of the dividing streamline (\hat{H}_0 and \hat{H}_1) are roughly approximated by σ_c and σ_1 , respectively. This approximation is only valid when $\sigma_c - \sigma_1$ is small because S85's theory does not account for the shear-layer depth. Thus, the present model simulation results agree with S85's finding that the critical nondimensional mountain height for high-drag state increases as the critical level height increases, although our explanation is based on the wave-ducting mechanism.

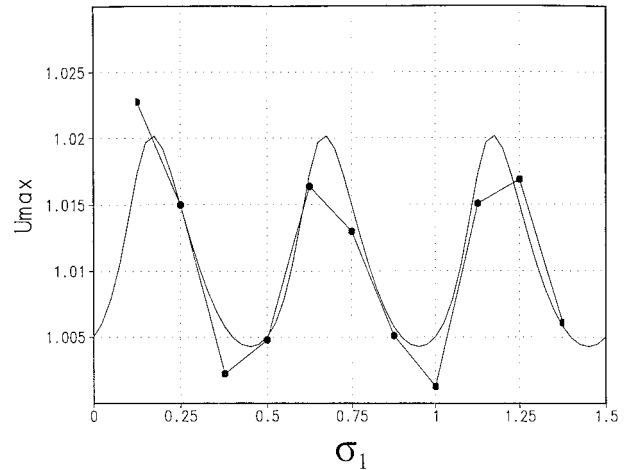


FIG. 4. The comparison of the magnitude of U_{\max} from the nonlinear numerical simulation (closed circles) with those from the linear analytical solution (solid line) for $h = 0.02$.

4. Nonlinear and critical level effects on the selection of high-drag states from linear wave duct modes

In this section, we will investigate why the high-drag state does not exist when $\sigma_1 = 0.675$ in our numerical simulations with a basic-state critical level and constant N (Fig. 1a). This is contradictory to the fact that the low-level disturbance is strongest when $\sigma_1 = 0.175 + n/2$ for flow with the same basic-state configuration, according to the linear wave-ducting theory developed in Part I.

In order to understand the dynamics of this absence of high-drag state at $\sigma_1 = 0.675$, we first perform a number of nonlinear numerical simulations with $h = 0.02$ and $Ri = 1$ and compare the results with those predicted by our linear wave-ducting theory. The nonlinearity at the lower boundary is insignificant because h is very small. Figure 4 shows the maximum nondimensional horizontal wind velocities ($U_{\max} = U_1 + u_{\max}$) over the lee surface, as predicted by both the present nonlinear numerical model and linear wave-ducting theory. It is obvious that these results agree fairly well, and the numerical simulations do show the peaks at $\sigma_1 = 0.175, 0.675, \text{ and } 1.175$. Note that there exists no high-drag state for this $h (0.02)$ in all nonlinear numerical simulations presented here. However, if h is increased slightly to 0.1, wave breaking occurs and produces a high-drag state when σ_1 is located at various heights according to the regime diagrams shown in Fig. 2. Notice that even though the lower layer is still linear, the flow becomes more and more nonlinear as the basic-state critical level is approached because the perturbation horizontal wind speed can easily exceed the basic-state wind speed (Bretherton 1966; Booker and Bretherton 1967). In other words, a slight increase of nonlinearity makes the selection of high-drag states from

the linear wave duct modes. That is, not every linear wave duct mode can develop into a high-drag state.

To understand the dynamics of this selection of high-drag states from the linear wave duct modes, we apply the linear wave-ducting theory developed in Part I to investigate the flow responses. Figures 5a–c show the horizontal perturbation wind fields from the linear analytical solution [Eq. (34) of Part I] with $Ri = 9.87$ and $h = 0.5$. The dimensional parameters used in these figures are $U_1 = 20 \text{ m s}^{-1}$, $U_3 = -0.02 \text{ m s}^{-1}$, $N_1 = N_2 = N_3 = 0.01047 \text{ s}^{-1}$, and $h = 955 \text{ m}$. Three cases with $z_1 = 0.175, 0.675, \text{ and } 1.175$ are shown in Figs. 5a–c, respectively. As can be inferred from the regime diagrams in Fig. 2, the flow is characterized as a high-drag state when $\sigma_1 = 0.175$ and 1.175 , and as a low-drag state when $\sigma_1 = 0.675$. In all cases, the low-level ($z < 0.175$) responses do exhibit almost identical patterns for all three cases. However, the responses between z_1 and z_c for cases with $z_1 = 0.175$ and 1.175 are very different from that with $z_1 = 0.675$. In Figs. 5a and 5c, there exists a region of positive horizontal perturbation wind right above this level, which has a magnitude about the same as that below $z = z_1$. Above this region of positive horizontal perturbation wind, there exists a much stronger negative horizontal perturbation wind, which actually induces two other critical levels at $z = 0.45, 0.57$ in the case with $z_1 = 0.175$ (Fig. 5d) and at $z = 1.45, 1.57$ in the case with $z_1 = 1.175$ (Fig. 5f). In fact, a closer inspection reveals that there are more new critical levels being induced near the basic-state critical level. The formation of these new critical levels may be explained by the decrease of vertical wavelength and the increase of the horizontal perturbation wind as one approaches the basic-state critical level from below, based on the linear theory (Bretherton 1966; Booker and Bretherton 1967). In fact, it can be shown that u oscillates and approaches ∞ near the basic-state critical level in a linear, steady-state flow over an isolated mountain (Smith 1986) and over a heat source (Lin 1987). In other words, the nonlinear effects become stronger as the basic-state critical level is approached. The corresponding vertical static stability profile at $x = 0$ from steady-state analytical solutions is also plotted in Figs. 5d and 5f. We find that there exists an unstable region between the lowest two new critical levels. This unstable region allows the wave duct mode to develop further into a high-drag state. The development of these two high-drag states ($z_1 = 0.175, 1.175$) from the corresponding linear wave duct modes has also been verified by the animation of the numerical results (not shown).

When $z_1 = 0.675$ (Fig. 5b), the flow response between z_1 and z_c is totally opposite from those in Figs. 5a and 5c. Above $z = z_1$, there exists a region of negative horizontal perturbation wind, which is capped by a much stronger positive perturbation wind. Further aloft, there likely exists an even stronger negative perturbation wind region with a much shorter vertical wavelength because it is closer to the basic-state critical level. Similar to

cases with $z_1 = 0.175$ and 1.175 , more new critical levels are also being induced, such as at $z = 1.08$ and 1.14 (Fig. 5e). However, according to the vertical profile of static stability, there exists a very stable layer ($N = 0.02 \text{ s}^{-1}$ at about $z = 1.03$) above the lower uniform wind layer. According to the linear wave-ducting theory, the static stability of the shear layer must be equal or less than that of the lower uniform wind layer. Thus, this highly stratified layer plays a role in suppressing the development of a high-drag state from the wave duct mode.

The formation of these new stable or unstable layers may be understood through the linear theory. The steady-state, small-amplitude equations in the shear layer used in deriving the above solutions are [Eqs. (5)–(8) of Part I],

$$U \frac{\partial u}{\partial x} + U_z w + \frac{\partial \phi}{\partial x} = 0, \quad (3)$$

$$\frac{\partial \phi}{\partial z} = b, \quad (4)$$

$$\frac{\partial u}{\partial x} + \frac{\partial w}{\partial z} = 0, \quad (5)$$

$$U \frac{\partial b}{\partial x} + N_z^2 w = 0. \quad (6)$$

The basic-state Brunt–Väisälä frequency in this layer is represented by N_2 . Differentiating (6) with respect to z and using (5) leads to

$$\frac{\partial \theta}{\partial z} = \left(\frac{N_2^2 \theta_0}{gU} \right) u. \quad (7)$$

In deriving the above equation, the relationship between the perturbation buoyancy (b) and the perturbation potential temperature, $b = g\theta/\theta_0$, has been used. The total Brunt–Väisälä frequency (N_t) can be obtained,

$$N_t^2 = \frac{g}{\theta_0} \frac{\partial \theta_t}{\partial z} = \frac{g}{\theta_0} \frac{\partial}{\partial z} (\bar{\theta} + \theta) = N_2^2 + \frac{g}{\theta_0} \frac{\partial \theta}{\partial z}, \quad (8)$$

where the subscript t denotes the total value of the flow variable. Note that the total Brunt–Väisälä frequency is denoted by $N^2(z)$ in Fig. 5. Now, we may substitute Eq. (7) into Eq. (8), which leads to

$$N_t^2 = N_2^2 \left(1 + \frac{u}{U} \right). \quad (9)$$

Therefore, the basic-state Brunt–Väisälä frequency (N_2^2) is modified by the strength of the nonlinearity, u/U . If U is positive in the shear layer, which is what we have in the present case, then N_t^2 is proportional to the perturbation wind velocity (u) and has the same sign. This explains the in-phase relationship of N_t^2 and u in Figs. 5d–f. In addition, N_t^2 increases as one approaches the basic-state critical level because u increases, too.

From the above discussions, we may conclude that if

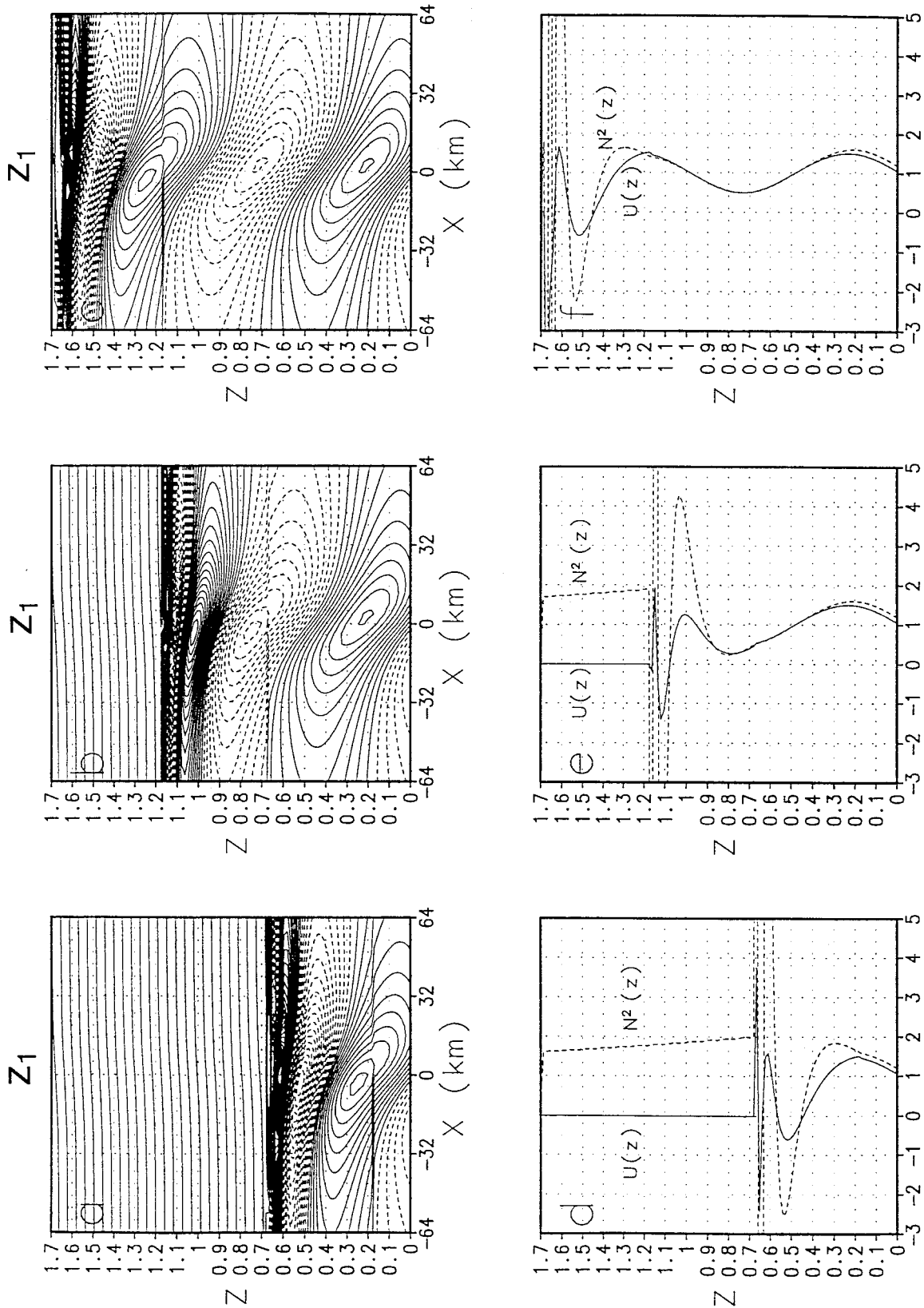


FIG. 5. The horizontal perturbation wind from the linear analytical solution [Eq. (34) of Part I] with $Ri = 9.87$ and $h = 0.5$ in the case with (a) $z_1 = 0.175$, (b) $z_1 = 0.675$, and (c) $z_1 = 1.175$. (d)–(f) The vertical profiles of horizontal wind (solid line) and static stability (dash line) at $x = 0$ for the results in (a)–(c), respectively. The dimensional parameters used in these figures are $U_1 = 20 \text{ m s}^{-1}$, $U_3 = -0.02 \text{ m s}^{-1}$, $N_1 = N_2 = N_3 = 0.01047 \text{ s}^{-1}$, and $h = 955 \text{ m}$. The nondimensional contour interval in (a)–(c) is 1.

a very stable layer is induced above σ_1 , then the linear wave duct mode tends to be suppressed and the flow cannot develop into a high-drag state. On the other hand, if an unstable layer is induced above σ_1 , then the linear wave duct mode may further develop into a high-drag state.

5. Implications of the nonlinear wave-ducting mechanism for the development of high-drag states

Because wave breaking is simply forced by the highly nonlinear lower boundary forcing and can be predicted by Long's (1953) solution in cases with uniform flow, we will focus on the stages after the occurrence of the "wave-induced critical level." According to Long's solution, when the nondimensional mountain height reaches its critical value ($h = 0.85$), there exists a wind reversal level at $z = \frac{3}{4}\lambda$, and the streamline in the region is almost vertical. The presence of this nearly neutral region, along with the presence of vertical shear, makes it possible for Ri to be less than one-quarter in the vicinity of the wave-induced critical level, which is a necessary condition for Kelvin-Helmholtz (shear or dynamical) instability to occur. According to our calculation in Fig. 7a of Part I, the reflectivity is very close to 1 when the static stability near the critical level becomes neutral. Note that the reflectivity in this region can be greater or less than 1 depending upon the value of Ri . The smaller Ri is, the larger the reflectivity.

Figure 6 shows the time sequence of horizontal wind fields during the development of a high-drag state for a flow with uniform wind and constant static stability. In this case, h is 1, which is characterized as a high-drag state because $h > 0.85$ (Miles and Huppert 1969; Lin and Wang 1996). Figure 6a shows the horizontal wind at the time just before flow stagnation aloft (wave breaking) occurs. At this stage, the flow pattern is close to that predicted by Long's solution and there exists no region with $Ri < 0.25$. Figure 6b shows the results shortly after the occurrence of wave breaking. Regions with local $Ri < 0.25$ are superimposed on the horizontal wind fields of Fig. 6. This wave breaking or turbulent mixing region is expanding downward and downstream due to strong nonlinear effects on the flow with low Ri near the critical level, as shown later (Fig. 8). Once wave breaking occurs, it may establish a wave duct below the turbulent mixing region (also called dead region in S85) and above the lee slope. Associated with the downward and downstream expansion of the turbulent mixing region, the wave duct becomes shallower (Fig. 6c). This is explained by the interaction of nonlinearity and the strong wave reflection, which will be shown later. When the depth of the wave duct is reduced, the wave will accelerate and propagate further downstream due to nonlinear advection, as shown in Lin and Wang (1996), and the trapping of wave energy between the turbulent mixing layer and lee slope (Part I). Note

that the expansion of the turbulent mixing region (where $Ri < 0.25$) provides a maintenance mechanism for the existence of the wave duct below it and above the lee slope, because the reflectivity in this region is about 1 according to the linear theory. Without this almost perfect reflector, the wave below it cannot be maintained and would lose most of its energy due to dispersion.

This development stage of severe downslope windstorms is supported by the nonlinear wave ducting mechanism since the nonlinear advection plays a significant role in broadening the turbulent mixing region. Note that the general linear criteria for wave duct to occur (Part I) may still provide a very useful guidance in identifying potential wave duct modes. Whether these linear wave duct modes can further develop into high-drag state or not depends upon the modification of the flow structure by nonlinear and critical level effects, as proved in last section. The stable layer below the turbulent mixing region is kept at a depth of about $\frac{1}{4}\lambda$ when the internal hydraulic jump propagates downstream. As first proposed by LT76, and generalized in Part I (see Fig. 5c of that paper), such a depth is optimal for a wave duct in cases with an almost neutral layer in the shear layer. Using a weakly nonlinear theory, Grimshaw and Smyth (1986) also showed that the initiation of a high-drag transitional flow begins with linear resonance. Once the nonlinear effects have been taken into consideration and the low-drag states (such as $\sigma_1 = 0.175 + n/2$) have been ruled out from the linear wave duct modes, the depth of the lower uniform flow layer for high-drag state (such as $\sigma_1 = 0.175 + n$), is consistent with what is predicted by linear wave-ducting theory.

As briefly reviewed in the introduction, Scinocca and Peltier (1993) have suggested that the drag and surface wind begin to increase in their second stage of the development of severe downslope windstorms. Figure 7 shows the time evolution of the normalized surface drag, the maximum horizontal wind velocity (U_{\max}) at the lee surface, and the minimum horizontal wind velocity (U_{\min}) aloft. This figure indicates that the flow stagnation aloft or wave breaking ($U_{\min} = 0$) occurs at about $Ut/a = 0$. The surface drag and U_{\max} at this time are about 2.5 and 2.2, respectively. The maximum horizontal wind velocity predicted by Long's solution (not shown) for this case ($h = 1$) is also 2.2. Note that the maximum wind velocity at the final time of the simulation ($Ut/a = 50.4$) is about 2.6, which is not much larger than the value 2.2 at $Ut/a = 10$. However, the surface drag keeps increasing until the quasi-mature state ($Ut/a = 40$) is reached. The quasi-mature state is defined as the time when the maximum surface wind over the lee slope reaches a quasi-steady value. The drag at the end of the simulation is about 3.9 ($Ut/a = 50.4$), although the strongest value is about 4.3 at $Ut/a = 40$. The increase in drag during this stage may be explained by the strong vertical wind associated with the internal hydraulic jump because the drag is proportional to the horizontal in-

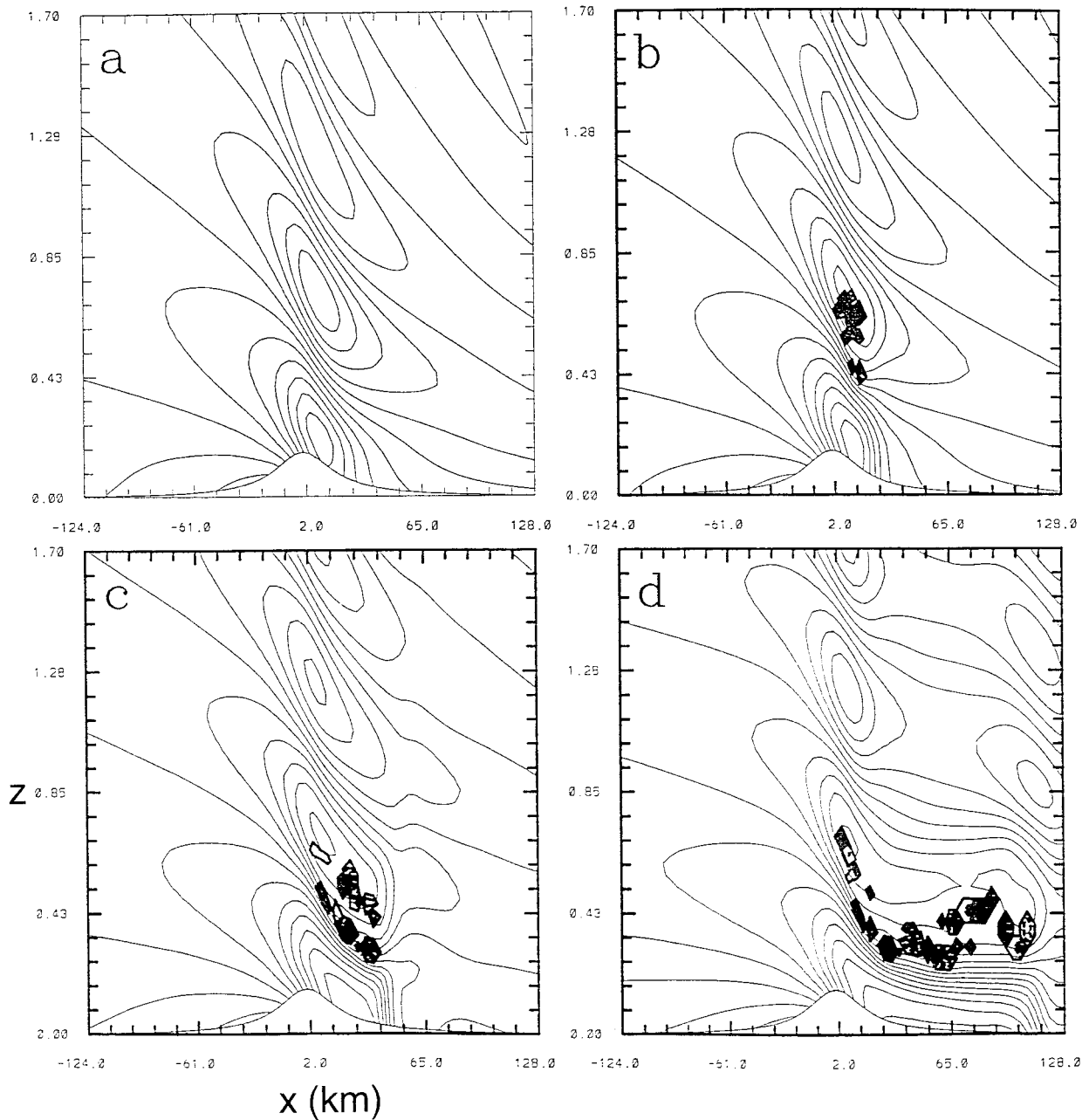


FIG. 6. Time sequence of horizontal wind field superimposed with the contours of local $Ri < 0.25$ (thick line) at nondimensional time $Ut/a =$ (a) 9.8, (b) 12.6, (c) 19.6, and (d) 50.4. The nondimensional contour interval is 0.2 and the maximum value near the surface in (c) is 2.4.

tegration of the vertical flux of horizontal momentum (uw). The increase of the strongest wind velocity from 2.2 at $Ut/a = 10$ to 2.6 at $Ut/a = 14$ is due to the nonlinear advection associated with strong horizontal wind over the lee slope (Lin and Wang 1996).

We now investigate the process responsible for the downward and downstream expansion of the turbulent mixing region during the development of a severe downslope windstorm. This will reduce the depth of the lower uniform wind layer or the wave duct. We hypothesize

that this flow behavior is due to the nonlinear effects. To verify this hypothesis, we perform both nonlinear and linear numerical simulations in a flow with a basic-state critical level at $\sigma = 0.75$ embedded in a shear layer between 0.25 and 0.75, which has a nearly neutral static stability ($N_2 = 0.0005 \text{ s}^{-1}$ in Fig. 1 of Part I). Note that $\sigma = 0.75$ is the height where wave breaking is usually observed in a uniform basic flow. This profile is used to mimic the environment at the beginning of the development stage of severe downslope windstorms. In

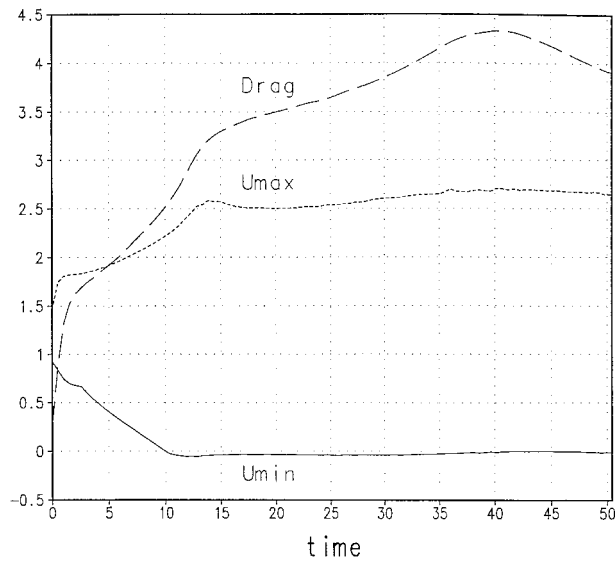


FIG. 7. Time evolution of normalized surface drag, maximum, and minimum horizontal wind velocities for the case in Fig. 6.

these simulations, we use $h = 0.5$ and $Ri = 0.1$. From the linear wave-ducting theory developed in Part I, linear wave duct modes exist at $\sigma_1 = 0.25 + n/2$ for this particular flow configuration (see case 3 of Table 1, Part I). From our nonlinear simulations (not shown), the linear wave duct modes of $\sigma_1 = 0.25 + n$ are able to develop into high-drag mode, but not those of $\sigma_1 = 0.25 + n/2$. Figures 8a and 8c show the potential temperature and vertical velocity fields, respectively, from the nonlinear simulation at $Ut/a = 10$. An internal hydraulic jump forms and propagates to $x = 38$ km, which is located at the head of the downstream-propagating disturbance over the lee slope. This is similar to the feature observed at this stage in the real atmosphere, in which a well-defined large-amplitude stationary disturbance is developed. Furthermore, an upstream-propagating bore is produced over the upslope at $x = 50$ km. Such an upstream bore is not observed in the uniform flow case because there exists no neutral region or critical level on the upstream side. The magnitude of the downstream horizontal velocity is about five times larger than the upstream value. In addition, according to the animation of the flow field (not shown), both the upstream and downstream waves are able to preserve their magnitudes while propagating, which provides strong evidence that the wave-ducting mechanism is at work, in addition to the evidence shown in earlier sections.

Figures 8b and 8d show the potential temperature and vertical velocity fields of the corresponding linear case. Apparently, without the inclusion of nonlinearity, the wave-breaking region does not expand downward to reduce the depth of the lower uniform wind layer. This, in turn, prohibits the formation of the severe downslope wind and internal hydraulic jump. These results verify our hypothesis that the downward and downstream ex-

pansion of the well-mixed region is due to nonlinear effects. Lin and Wang (1996) also investigated the importance of nonlinearity in the development of severe downslope winds by calculating the nonlinear terms for a uniform flow over a bell-shaped mountain with $h = 1$. They found that, in the absence of nonlinear effects, the downstream propagating jump is not able to develop. The present results are consistent with their finding. The case we show here is with $h = 0.5$, which provides enough nonlinearity for the linear ducted wave mode to develop into a high-drag state. Note that this nondimensional mountain height is less than the critical value for the occurrence of a high-drag state in a uniform basic flow. However, the downstream propagating internal hydraulic jump also cannot form in the absence of nonlinearity for such a wave duct mode, even though the wave amplification is observed from a linear simulation (Figs. 8b and 8d).

6. Concluding remarks

In this study, we tried to 1) clarify the discrepancies among various studies of severe downslope windstorms, 2) investigate the nonlinear and critical-level effects on the selection of linear wave duct modes into high-drag states, and 3) apply the nonlinear wave-ducting mechanism to the development of high-drag states associated with severe downslope windstorms. Both the linear wave-ducting theory (Part I) and a nonlinear numerical model were used to investigate the problem.

We found that the discrepancies among earlier studies of severe downslope windstorms are caused by the use of the critical level height (σ_c), instead of the depth of the low-level uniform wind layer (σ_1), as an indicator to determine the optimal conditions for the occurrence of high-drag states. Our explanation is that once the wave breaking occurs, it induces a critical level and establishes a flow configuration favorable for wave ducting to exist in the lower uniform wind layer. Thus, the low-level flow response is much more sensitive to the lower-layer height than to the critical-level height. This sensitivity is due to the fact that the phase of the reflected waves is primarily determined by \tilde{z}_1 as found in Part I. This, in turn, implies that using the depth of the lower uniform wind layer is a better indicator than the critical-level height to determine the optimal conditions for the occurrence of high-drag states. The predictions from CP84, DK87, BP88, and our present model, for both high- and low-drag states by using σ_1 as the control parameter are consistent. Thus, the use of the lower uniform wind-layer depth appears to better follow a more consistent pattern. This also provides evidence that the wave-ducting mechanism plays an important role in producing high-drag states.

Flow regimes of high- and low-drag states for a two-dimensional, nonrotating flow with a basic-state critical level and uniform N over a two-dimensional mountain were also determined as functions of nondimensional

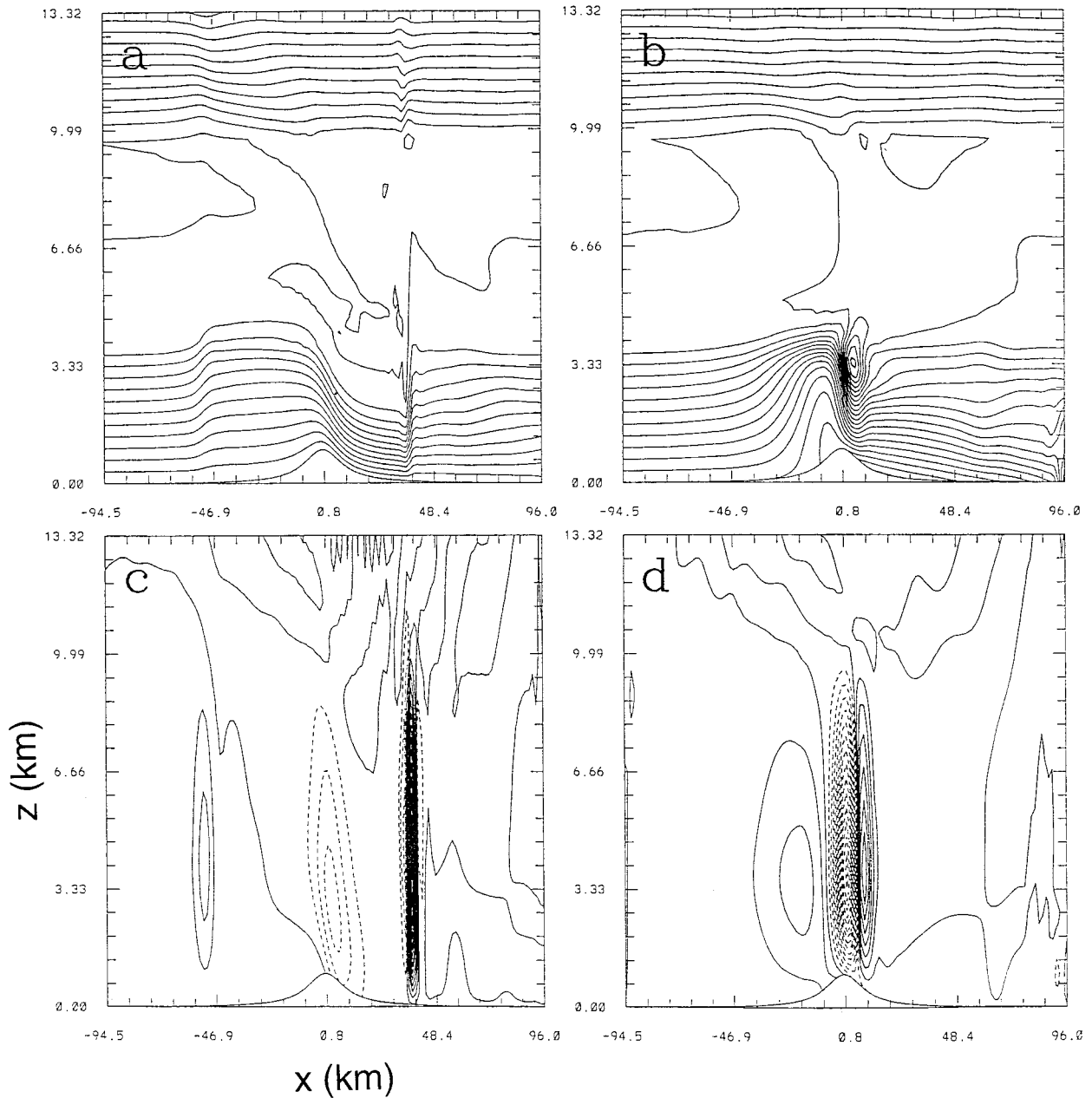


FIG. 8. (a) Potential temperature field from nonlinear numerical simulations with $Ri = 0.1$ and $h = 0.5$. (b) Same as (a) except from linear numerical simulations. (c) and (d) Same as (a) and (b), respectively, except for vertical velocity field. The contours in (a) and (b) are from 273 to 298 K and from 268 to 297 K, respectively. The contour interval is 1 K in both (a) and (b). The contours in (c) are from -2.7 to 10.8 m s^{-1} with an interval of 0.9 m s^{-1} , and are from -14 to 6 m s^{-1} with an interval of 1 m s^{-1} in (d).

mountain height (\bar{h}), Ri , and nondimensional lower-layer depth ($\bar{\sigma}_1$) by a series of numerical experiments. We found that 1) the critical \bar{h} for the high-drag state increases as Ri increases when $\bar{\sigma}_1$ is fixed, 2) the critical \bar{h} for the high-drag state increases as $\bar{\sigma}_1$ increases from $0.175 + n$ to $1.175 + n$ when Ri is fixed, and 3) the low-level response repeats periodically at one vertical wavelength. This also provides additional evidence that the wave ducting has played an important role in gen-

erating high-drag states. The present model simulation results agreed with S85's finding that the critical \bar{h} for the high-drag state increases as the critical-level height increases when the shear-layer depth is small, although our explanation was based on the wave-ducting mechanism, which applied to the development stage of a severe downslope windstorm, instead of at the mature stage. The selection of high-drag states ($\bar{\sigma}_1 = 0.175 + n$) from the linear wave duct modes ($\bar{\sigma}_1 = 0.175 + n/2$)

is due to the nonlinear and critical-level effects. In other words, an increase of nonlinearity makes the selection of high-drag states from the linear wave duct modes. That is, not every linear wave duct mode can develop into a high-drag state. We found that if a very stable layer is induced above $\bar{\sigma}_1$ (such as $\bar{\sigma}_1 = 0.675 + n$), then the linear wave duct mode tends to be suppressed and the flow cannot develop into a high-drag state because the wave-ducting structure is destroyed. On the other hand, if an unstable layer is induced above $\bar{\sigma}_1$ (such as $\bar{\sigma}_1 = 0.175 + n$), then the linear wave duct mode may further develop into a high-drag state.

It was found that once the wave breaking occurs, it may establish a wave duct below the lower boundary of the turbulent mixing region (also called the "dead region" in S85) and the lee slope. Strong nonlinear effects on this turbulent mixing region coupled with low Ri force this region to expand downward and downstream. Associated with this downward and downstream expansion of the turbulent mixing region, the wave duct becomes shallower. This is explained by the interaction of nonlinearity and the strong wave reflection. When the depth of the wave duct is reduced, the disturbance will accelerate and propagate further downstream as a hydraulic jump due to nonlinear advection, as shown in Lin and Wang (1996), and the trapping of wave energy between the turbulent mixing layer and lee slope (Part I). Note that the expansion of the well-mixed region (where $Ri < 0.25$) helps maintain the wave duct below it, because the reflectivity in this region is about 1 according to the linear wave-ducting theory (Part I). Without this almost perfect reflector, the wave below it cannot be maintained due to dispersion. This development stage of high-drag or severe wind state is supported by the nonlinear wave-ducting mechanism since the nonlinear advection plays a significant role in broadening the turbulent mixing region. At the mature stage of a severe downslope windstorm, the high-drag state is maintained by the hydraulic mechanism, as proposed by S85 and confirmed numerically by DK87 and BP88.

The development stage of severe downslope windstorm proposed in this study is related to the second and third stages proposed by Scinocca and Peltier (1993). In some sense, this is also related to the partial reflection mechanism (Klemp and Lilly 1975) and the resonant amplification mechanism (Peltier and Clark 1979; CP84). However, our explanation is based on the nonlinear wave-ducting mechanism. There is no conflict between the nonlinear wave-ducting mechanism and the hydraulic mechanism proposed (S85) because they play different roles at different stages of severe downslope windstorms. This is why S85's theory offered an excellent consistency analysis of a severe wind configuration, whereas our nonlinear wave-ducting mechanism may provide help in making a prediction of when a high-drag state will occur.

In order to apply the present nonlinear wave-ducting mechanism derived from an idealized three-layer at-

mosphere to predict severe downslope windstorms in the real atmosphere, a more realistic and complicated basic-state environment needs to be considered. For example, in the arguments presented in this paper, we have assumed that z_1 for maximum low-level responses is independent of Ri. Strictly speaking, this assumption is valid only when N is uniform or $N_2/N_1 \ll 1$, according to the linear wave-ducting theory developed in Part I. Thus, it is important to examine the nonlinear wave-ducting mechanism in a more general three-layer atmosphere.

Acknowledgments. This work is supported by NSF Grant ATM-9224595. The authors wish to thank Drs. R. B. Smith, M. L. Kaplan, S. E. Koch, G. S. Janowitz, and three anonymous reviewers for valuable comments on the manuscript. Proofreading of the manuscript by Dr. R. P. Weglarz and Mr. Bo-Wen Shen are appreciated. Part of the computation was performed on the CRAY C90 at the North Carolina Supercomputer Center, and on the FOAM^v workstation cluster at NCSU, which is funded by IBM.

REFERENCES

- Bacmeister, J. T., and R. T. Pierrehumbert, 1988: On high-drag states of nonlinear stratified flow over an obstacle. *J. Atmos. Sci.*, **45**, 63–80.
- Booker, J. R., and F. P. Bretherton, 1967: The critical layer for internal gravity waves in a shear flow. *J. Fluid Mech.*, **27**, 513–539.
- Bretherton, F. P., 1966: The propagation of groups of internal gravity waves in a shear flow. *Quart. J. Roy. Meteor. Soc.*, **92**, 466–480.
- Clark, T. L., and W. R. Peltier, 1984: Critical level reflection and the resonant growth of nonlinear mountain waves. *J. Atmos. Sci.*, **41**, 3122–3134.
- Durrant, D. R., 1986: Another look at downslope windstorms. Part I: On the development of analogs to supercritical flow in an infinitely deep, continuously stratified fluid. *J. Atmos. Sci.*, **43**, 2527–2543.
- , 1993: Comments on "On the Richardson number dependence of nonlinear critical-layer flow over localized topography." *J. Atmos. Sci.*, **50**, 3029–3033.
- , and J. B. Klemp, 1982: The effects of moisture on trapped mountain lee waves. *J. Atmos. Sci.*, **39**, 2490–2506.
- , and —, 1983: A compressible model for the simulation of moist mountain waves. *J. Atmos. Sci.*, **40**, 2341–2361.
- , and —, 1987: Another look at downslope winds. Part II: Nonlinear amplification beneath wave-overturning layers. *J. Atmos. Sci.*, **44**, 3402–3412.
- Gal-Chen, T., and R. C. Somerville, 1975: On the use of a coordinate transformation for the solution of the Navier–Stokes equations. *J. Comput. Phys.*, **17**, 209–228.
- Grimshaw, R. H., and N. Smyth, 1986: Resonant flow of a stratified fluid over topography. *J. Fluid Mech.*, **169**, 429–464.
- Houghton, D. D., and A. Kasahara, 1968: Nonlinear shallow fluid flow over an isolated ridge. *Commun. Pure Appl. Math.*, **21**, 1–23.
- Klemp, J. B., and D. K. Lilly, 1975: The dynamics of wave-induced downslope winds. *J. Atmos. Sci.*, **32**, 320–339.
- Laprise, R. J., and W. R. Peltier, 1989a: The linear stability of nonlinear mountain waves: Implications for the understanding of severe downslope windstorms. *J. Atmos. Sci.*, **46**, 545–564.
- , and —, 1989b: On the structural characteristics of steady

- finite-amplitude mountain waves over bell-shaped topography. *J. Atmos. Sci.*, **46**, 586–595.
- Lilly, D. K., 1978: A severe downslope windstorm and aircraft turbulence induced by a mountain wave. *J. Atmos. Sci.*, **35**, 59–77.
- , and E. J. Zipser, 1972: The front range windstorm of 11 January 1972—A meteorological narrative. *Weatherwise*, **25**, 56–63.
- Lin, Y.-L., 1987: Two-dimensional response of a stably stratified shear flow to diabatic heating. *J. Atmos. Sci.*, **44**, 1375–1393.
- , and T.-A. Wang, 1996: Flow regimes and transient dynamics of two-dimensional stratified flow over an isolated mountain ridge. *J. Atmos. Sci.*, **53**, 139–158.
- Lindzen, R. S., and K.-K. Tung, 1976: Banded convective activity and ducted gravity waves. *Mon. Wea. Rev.*, **104**, 1602–1617.
- Long, R. R., 1953: Some aspects of stratified fluids. Part I: A theoretical investigation. *Tellus*, **5**, 42–58.
- , 1954: Some aspects of the flow of stratified fluids. Part II. Experiments with a two fluid system. *Tellus*, **6**, 97–115.
- Miles, J. W., and H. E. Huppert, 1969: Lee waves in a stratified flow. Part 4: Perturbation approximations. *J. Fluid Mech.*, **35**, 497–525.
- Peltier, W. R., 1993: Reply. *J. Atmos. Sci.*, **50**, 3034–3040.
- , and T. L. Clark, 1979: The evolution and stability of finite-amplitude mountain waves. Part II: Surface wave drag and severe downslope winds. *J. Atmos. Sci.*, **36**, 1498–1529.
- , and —, 1980: Reply. *J. Atmos. Sci.*, **37**, 2122–2125.
- , and —, 1983: Nonlinear mountain waves in two and three spatial dimensions. *Quart. J. Roy. Meteor. Soc.*, **109**, 527–548.
- Queney, P., 1948: The problem of air flow over mountains: A summary of theoretical studies. *Bull. Amer. Meteor. Soc.*, **29**, 16–26.
- Rottman, J. W., and R. B. Smith, 1989: A laboratory model of severe downslope winds. *Tellus*, **41A**, 401–415.
- Scinocca, J. F., and W. R. Peltier, 1991: On the Richardson number dependence of nonlinear critical-layer flow over localized topography. *J. Atmos. Sci.*, **48**, 1560–1572.
- , and —, 1993: The instability of Long's stationary solution and the evolution toward severe downslope windstorm flow. Part I: Nested grid numerical simulations. *J. Atmos. Sci.*, **50**, 2245–2263.
- Smith, R. B., 1979: The influence of mountains on the atmosphere. *Advances in Geophysics*, Vol. 21, Academic Press, 87–230.
- , 1985: On severe downslope winds. *J. Atmos. Sci.*, **42**, 2597–2603.
- , 1986: Further development of a theory of lee cyclogenesis. *J. Atmos. Sci.*, **43**, 1582–1602.
- , and Y.-L. Lin, 1982: The addition of heat to a stratified airstream with application to the dynamics of orographic rain. *Quart. J. Roy. Meteor. Soc.*, **108**, 353–378.
- Wang, T.-A., and Y.-L. Lin, 1998: Wave ducting in a stratified shear flow over a two-dimensional mountain. Part I: General linear criteria. *J. Atmos. Sci.*, **56**, 412–436.
- Weglarz, R. P., 1994: Three-dimensional geostrophic adjustment of homogeneous and continuously stratified atmosphere with application to the dynamics of midlatitude jetstreaks. Ph.D. dissertation, North Carolina State University, Raleigh, NC, 414 pp.